PHYSICS AND CHEMISTRY OF SOLID STATE
V. 25, No. 1 (2024) pp. 178-184
Section: Chemistry

DOI: 10.15330/pcss.25.1.178-184

Vasyl Stefanyk Precarpathian National University

ФІЗИКА І ХІМІЯ ТВЕРДОГО ТІЛА
Т. 25, № 1 (2024) С. 178-184
Хімічні науки

PACS: 62.20.de; 81.40.Jj ISSN 1729-4428

Khrystyna Khrushchyk[1,2], Adrian Barylski[2], Krzysztof Aniolek[2], Malgorzata Karolus[2], Lidiya Boichyshyn[1]

Mechanical properties of amorphous metal alloy $Al_{87}(Ni,Fe)_8(REM)_5$ system as a result of short-term annealing

[1]*Ivan Franko National University of Lviv, Lviv, Ukraine,*
[2]*University of Silesia in Katowice, Katowice, Poland, khrystyna.khrushchyk@us.edu.pl*

The phase transition temperatures for amorphous metals based on aluminum $Al_{87}(Ni,Fe)_8(REM)_5$ system were determined by differential scanning calorimetry (DSC). The mechanisms of formation and growth of nanocrystals in an amorphous matrix were predicted using kinetic models (Matusita model). It was found that after annealing at the temperature of stable nanocrystalline growth, an X-ray amorphous structure with a volume fraction of disordered nanocrystalline phases of solid state of Al(X), $GdFe_2$, $AlFe_2Ni$, $GdFe_2$ for the amorphous metal alloy (AMA) $Al_{87}Y_4Gd_1Ni_4Fe_4$ alloy and microcrystalline phases of solid state of Al(X), $GdFe_2$ $AlFe_2Ni$ for the $Al_{87}Gd_5Ni_4Fe_4$ alloy are formed, which significantly affects the mechanical properties of the $Al_{87}(Ni,Fe)_8(REM)_5$ system. The effect of annealing on the mechanical properties of amorphous aluminum-based alloys was investigated using Oliver-Pharr and Young's modulus methods it was found that thermal modification of AMAs: $Al_{87}Gd_5Ni_4Fe_4$ as a result of heat treatment of AMAs from 5 to 15 min., the microhardness increases from 0.20 GPa to 2.75 GPa, and when heat treated for 60 min at a temperatures of $T_3 = 645\pm5$ K, 647 ± 5 K, it decreases to 0.35 GPa and 0.45 GPa, respectively.

Keywords: amorphous metal alloys based on aluminum, differential scanning calorimetry, microhardness, nanocrystallization, Young's modulus.

Received 02 November 2023; Accepted 12 February 2024.

Introduction

Amorphous alloys have a valuable set of mechanical properties. First and foremost, they are characterized by a combination of high hardness and strength [1-3]. The microhardness of a material characterizes the strength of the bond between atoms in the structure, so changes in microhardness indicate changes in the structure of the amorphous phase. Therefore, it is obvious that an increase in microhardness during annealing is associated with both free volume reduction and ordering processes.

The main requirement for use as structural materials is structural stability at high temperatures. It is known that AMA based on aluminum mainly crystallizes in three stages when heated. Doping with *p*-, *d*- and *f*-elements changes the temperature and number of crystallization stages. The first stage is nanocrystallization, which is comprehensively studied and described by many authors [4-9].

Thus, the authors [4] showed that annealing at temperatures 50-100 K lower than the nanocrystallization temperature results in the delamination of the amorphous phase into two different compositions: AF1 is enriched with atoms of *d*-elements, AF2 is enriched with atoms of *f*-elements. The temperature of nanocrystallization depends on the quantitative ratio and the nature of the alloy components: after heating, aluminum nanocrystals are formed at higher temperatures, $Al_{87}Ni_{10}Gd_3$ [10] at T= 444 K; $Al_{87}Gd_5Ni_8$ [11] at T= 510 K, $Al_{90}Ni_3Gd_7$ [10] at T= 437 K, $Al_{85}Y_{10}Ni_5$ [11] at T= 524 K, $Al_{86}Ni_9La_5$ [9] at T= 522 K, $Al_{85}Ni_5Y_8Co_2$ [12]at T= 556 K, $Al_{87}Gd_5Ni_4Fe_4$ [11] at T= 558 K, $Al_{87}Y_4Gd_1Ni_4Fe_4$ [11] at T= 543 K.

As can be seen in some alloys based on Al,

crystallization occurs much easier due to the presence of hardened crystal cores with an average arrangement of atoms [13–14]. The authors of [11] reported on crystallization in some amorphous aluminum alloys at temperatures significantly lower than their crystallization temperatures. At a high particle density (10^{22}–10^{23} m^{-3}) of hardened nuclei, their further growth can be stopped due to the reduction of diffusion layers that regulate crystal growth. The following can occur at grain boundaries: (I) one layer of dopants; (II) clean grain boundaries (no dopant layer); (III) two-layered; (IV) multilayer (more than two layers of atoms). In the case of transformations of amorphous structures, it is necessary to take into account the following processes, which are different in nature: 1) diffusion jump of an atom into a free node in the first three coordination spheres; 2) atom desorption from the open surface; 3) adsorption of an atom on an open surface; 4) release of atoms from closed cavities.

All these processes will affect the numerical values of the kinetic parameters by which the crystallization processes are analyzed. The crystallization kinetics of vitreous materials can be described by three kinetic parameters, namely: crystallization activation energy (1); the Avrami index, which reflects the mechanism of crystal nucleation and growth (2); the frequency factor characterizing the maximum possible speed of the process (3) [15-21]. The purpose of this work is to study the influence of the duration of isothermal annealing of AMAs at the temperatures of the second stage of crystallization and alloying additions in five amorphous alloys: $Al_{87}Y_5Ni_8$, $Al_{87}Gd_5Ni_8$, $Al_{87}Y_4Gd_1Ni_8$, $Al_{87}Y_4Gd_1Ni_4Fe_4$ and $Al_{87}Gd_5Ni_4Fe_4$, on the kinetic parameters and products of their crystallization.

I. Objects and methods of research

The object of the tests were AMAs alloys with the composition: $Al_{87}Gd_5Ni_4Fe_4$ and $Al_{87}Y_4Gd_1Ni_4Fe_4$ in the form of ribbons with a thickness and width of 20-25 μm and 3 mm, respectively, which were obtained at the Institute of Metallurgy of the Ukrainian Academy of Sciences (Kyiv) by melt spinning method in a helium atmosphere on a copper drum rotating at a speed of ~30 m/s. The melt was prepared from pure metals and binary compounds $REAl_3$ (RE = Y, Gd). The purity of the starting metals was as follows: Al (99.999 wt.%), Ni (99.99 wt.%), Y (99.96 wt.%), Gd (99.96 wt.%) and Fe (99.99 wt.%). Rare earth metals in the form of binary compounds Al_3Gd and Al_3Y were mainly obtained by the method of arc melting from metals of the same purity.

The following experimental techniques were used to study changes in physical and chemical properties due to heat treatment:

Differential scanning calorimetry (DSC, Perkin-Elmer Pyris 1) with different heating rates of 5, 10, 20 K/min of samples. The obtained data were evaluated using the standard Pyris program. X-ray diffraction method was used for samples in their initial state and annealed at T_3 (second peak) for different times of 5, 15, 30, 45, and 60 min. The X-ray diffraction analysis was performed by using the PANalytical Empyrean Diffractometer with Cu-Kα radiation (λ $K\alpha_1$ = 1.5418 Å) and the PIXcell detector. Phase analysis was done basing on the HighScore Plus PANalytical software integrated with the ICDD PDF4 + 2016 crystallographic database [22-23]. High resolution electron microscopy (HREM, JEM 3010). HREM observations were used to confirm (or not confirm) the conclusions reached by DSC and X-ray methods. Static tensile testing was carried out on an INSTRON 5982 testing machine. The traverse speed of the machine during testing was 1 mm/min. Tensile curves were recorded in the coordinate system: stress σ - relative strain ε. Mechanical properties of AMAs were investigation using Micro Combi Tester (Micro Scratch + Microindentation) MCT3 (Oliver-Pharr method, type of indentors: Berkovich and material: Diamond; Indentation Parameters: max load: 100.00 mN, loading/ unloading rate: 200.00 mN/min, pause: 10.0 sec).

The mechanisms of the formation of the crystalline phase in AMAs were established using the Matusit model [24]:

$$\ln[-\ln(1-\alpha)] = -n\ln(\beta) - 1.052\frac{mE_\alpha}{RT} + C, \qquad (1)$$

where α is the volume fraction of crystalline phases; n is Avrami's index; m is the dimension growth parameter, C-constant. The Matusita model provides additional useful information about the mechanism and direction of growth during the crystallization of AMAs based on the relationship between the Avrami exponent n and the dimension growth parameter *m* [21]:

$$n = b + pm, \qquad (2)$$

where *b* is a parameter characterizing the nucleation rate; *p* is a parameter characterizing the type of transformation. Correspondence of the numerical values of the parameters *m*, *p* and *b* to the features of the growth of crystalline phases in the amorphous matrix [25-27].

II. Results and Discussion

In fig. 1, there is presented the example of process of heating results (DSC) obtained for $Al_{87}Y_4Gd_1Ni_4Fe_4$ alloy. During the heating process carried out DSC in aluminum-based alloys, a three-stage crystallization was observed, leading to the formation of α-Al, phases and metastable Al-(Y, Gd) phases. One can see that the AMAs based on aluminum undergoes three-stage crystallization leading to the formation of α-Al, and metastable phases Al-(Y,Gd).

The annealing temperature in further research steps, was determined from the third crystallization step (T_3) at the second DSC maximum in the temperature range 323–900 K with a heating rate of β = 20 K/min.

From fig. 1 (b) it can be seen that the crystallization temperatures increase as the heating rate (β) increases. AMAs $Al_{87}Gd_5Ni_4Fe_4$ and $Al_{87}Y_4Gd_1Ni_4Fe_4$ were annealed for 5, 15, 30, 45, and 60 min. at temperatures specific (determined from DCS analysis) to each sample: 645±5, 647±5 K, respectively. The rate of heating the furnace to the selected temperature was about 17-20 K/min.

Fig. 2 shows the dependence of the change in the

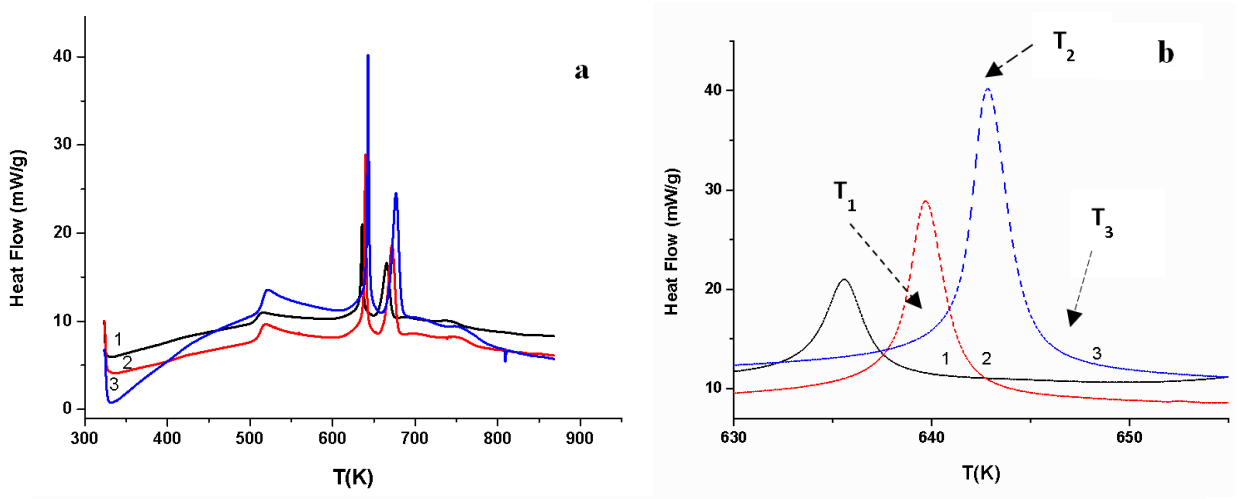

Fig. 1. (a) DSC-curves (β =10 (1 – black curve), 15 (2 – red curve), 20 (3 – blue curve) K/min) of an example amorphous metal alloys of $Al_{87}Y_4Gd_1Ni_4Fe_4$ in the temperature range 323–900 K.
T_1 – temperature of nucleation, T_2 – temperature of growth and T_3 – temperature of formation of α-Al nanocrystals; (b) DSC-curves for AMAs $Al_{87}Y_4Gd_1Ni_4Fe_4$ in the temperature range of 695-615 K (second peak of crystallization) at different heating rates (β) 1-10 K/min, 2-15 K/min, 3-20 K/min.

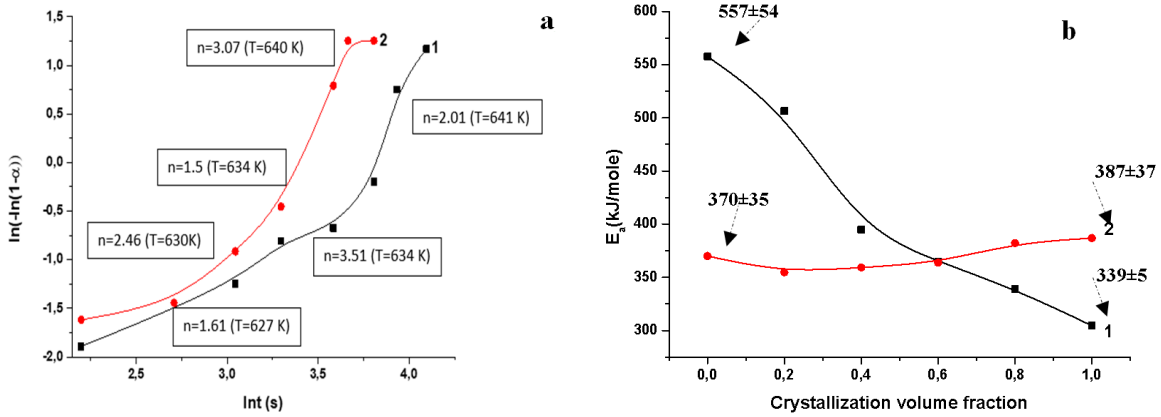

Fig. 2. The dependencies of ln[−ln(1−α)] on lnt at different volume fraction of crystalization for AMAs:
(a) 1 – $Al_{87}Y_4Gd_1Ni_4Fe_4$, 2 – $Al_{87}Gd_5Ni_4Fe_4$; (b) The dependencies of local crystallization activation energy on crystalization volume fraction for the AMAs for second peak of crystallization:
1 – $Al_{87}Gd_5Ni_4Fe_4$, 2 – $Al_{87}Gd_1Y_4Ni_4Fe_4$.

degree of crystallinity on the annealing duration in the coordinates ln[-ln(1-α)] versus ln t. As can be seen, the value of *n* (crystallization rate) of AMA for the $Al_{87}Y_4Gd_1Ni_4Fe_4$ alloy increases from 1.61 to 2.01. That is, the heating time and temperature increase to 647±5 K do not significantly affect the value of n. This can be explained by the model of the free volume formed by Y atoms (r = 0.181 nm) with the main component of Al (r = 0.143 nm). The complete replacement of Y by Gd in the $Al_{87}Gd_5Ni_4Fe_4$ alloy leads to an increase in the crystallization rate even at T = 645±5 K, from n = 2.46 to n = 3.01. Alloying AMA $Al_{87}Y_4Gd_1Ni_8$ with 4 at.% Fe leads to an increase in the crystallization temperature by 35-40 K [5, 15] and a decrease in the n value with increasing heating temperature. Iron atoms form diffusion layers that inhibit the growth of crystals in the volume of the amorphous matrix. As the heating temperature increases, the phase boundary shifts due to the diffusion of Al atoms, and the growth rate of the crystalline phase increases accordingly. These assumptions are illustrated by the HREM image (Fig. 5). The areas of the interface are highlighted in Fig. 5.

The crystal growth is diffusion-controlled [3, 5, 15], as indicated by the decrease in the growth rate due to the depletion of the interface between the amorphous matrix/crystal and the atoms of the main component. Thus, the process leads to an increase in the number of α-Al nanocrystals (average diameter of α-Al nanocrystals for $Al_{87}Gd_5Ni_4Fe_4$ at annealing for 60 min. at T_3 =645±5K is 35 ± 7 nm, for $Al_{87}Y_4Gd_1Ni_4Fe_4$ at annealing for 60 min. at T_3 =647±5 K is 25 ±5 nm [5, 15]) but not in their size, resulting in a corresponding increase in the microhardness of the alloy (Fig. 3b) for AMA $Al_{87}Gd_5Ni_4Fe_4$, when heat treated from 5 to 45 minutes. With further heating, the amorphous-nanocrystalline composite microstructure is transformed into a fully crystalline state with the formation of intermediate or final equilibrium phases [29, 30].

As a result of heat treatment of $Al_{87}Gd_5Ni_4Fe_4$ and $Al_{87}Y_4Gd_1Ni_4Fe_4$ AMAs for 5-60 min, the following structural transformations occur:

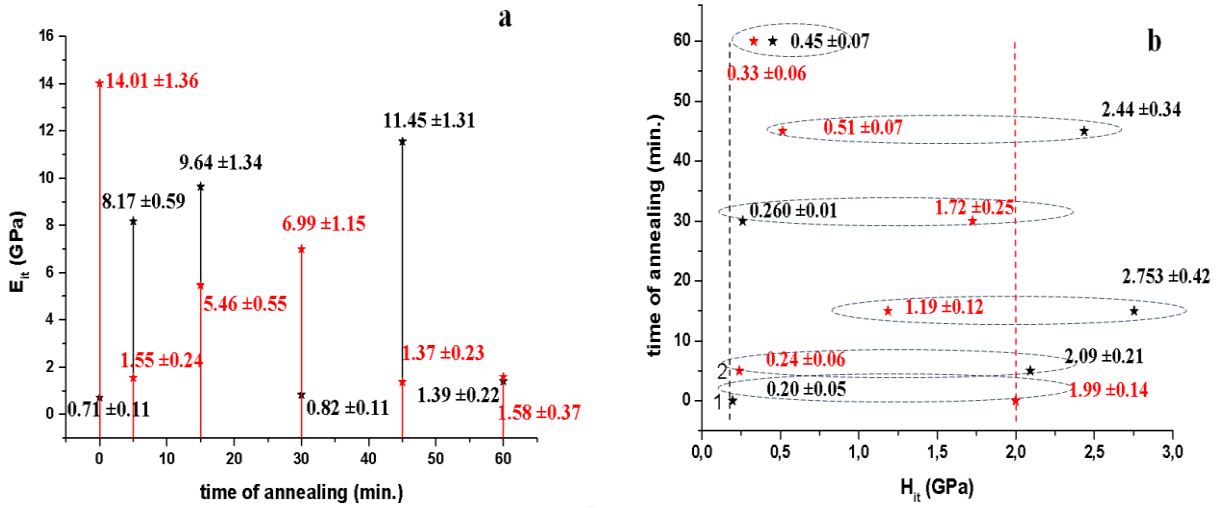

Fig. 3. Changes in values (a) modulus of Young and (b) microhardness due to annealing for AMAs: 1 – $Al_{87}Gd_5Ni_4Fe_4$ (black points), 2 – $Al_{87}Y_4Gd_1Ni_4Fe_4$ (red points).

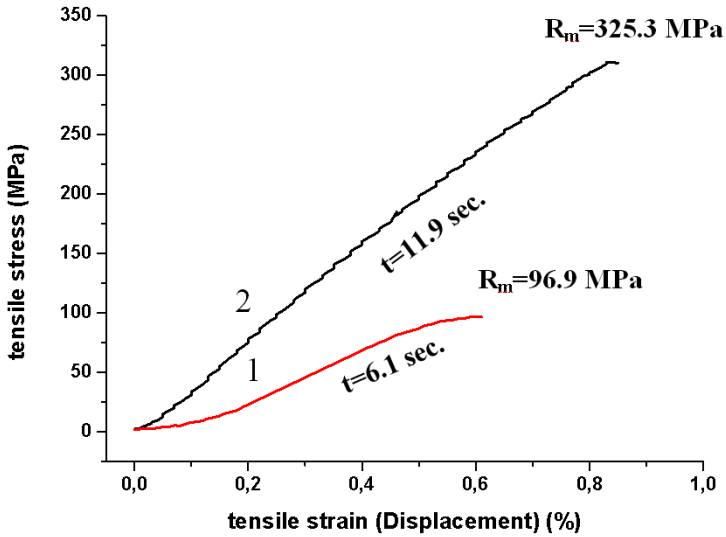

Fig. 4. The graphs from the tensile test for initial AMA: 1 – $Al_{87}Gd_5Ni_4Fe_4$, 2 – $Al_{87}Y_4Gd_1Ni_4Fe_4$.

amorph $Al_{87}Gd_5Ni_4Fe_4$ → nano(α-Al(REE)-rich → Al(X)+$GdFe_2$+$AlFe_2Ni$
amorph $Al_{87}Y_4Gd_1Ni_4Fe_4$ → nano(Al(X))+nano($GdFe_2$)+nano($AlFe_2Ni$)

The microhardness of the nanocrystalline and crystalline alloys of the AMAs system obtained from the initial AMAs depends on the stability of the amorphous matrix in the intercrystalline space [28]. Obviously, its significant increase is associated with interatomic interaction and changes in free volumes in the quasicrystalline structure. The change in microhardness with the annealing time of AMAs is shown in Fig. 3(b); this dependence is non-monotonic: thermal modification of AMA $Al_{87}Gd_5Ni_4Fe_4$ as a result of AMAs heat treatment from 5 to 15 min, the microhardness increases from 0.20 to 2.75 GPa. For $Al_{87}Y_4Gd_1Ni_4Fe_4$, the microhardness values decrease after annealing, which can be explained by the model of the free volume, which is formed by the atom Y (r = 0.181 nm) with the main component Al (r = 0.143 nm). At higher annealing temperatures (645, 647 K) and longer annealing times (60 min.), the nucleation processes are significantly inhibited and the volume fraction of the nanocrystalline phase increases mainly due to grain growth [3, 13], which leads to a decrease in microhardness with values of 0.3-0.5 GPa.

The tensile strength for aluminum alloys in the amorphous state state is approximately 800 MPa, and in the partially crystallized state after isothermal heat treatment – 1500 MPa. The tensile strength of pure crystalline Al (99.99%) is 45 MPa. The tensile test characterizes the properties of AMA the tensile strength, as shown in fig. 4 shows that this indicator is 3.4 times higher (fig. 4) for AMA $Al_{87}Y_4Gd_1Ni_4Fe_4$ compare to the $Al_{87}Gd_5Ni_4Fe_4$.

Fig. 5 shows the HRTEM-image of $Al_{87}Gd_5Ni_4Fe_4$ AMAs after a 60 min. annealing at the temperature of the end of the second stage of AMAs crystallisation. Crystals of intermetallic compounds of various different compositions are formed in the alloy volume [31]. It can be seen that annealing for 60 min. results in almost complete crystallisation of AMAs with a residual amorphous matrix (Fig. 5). As can be seen from the

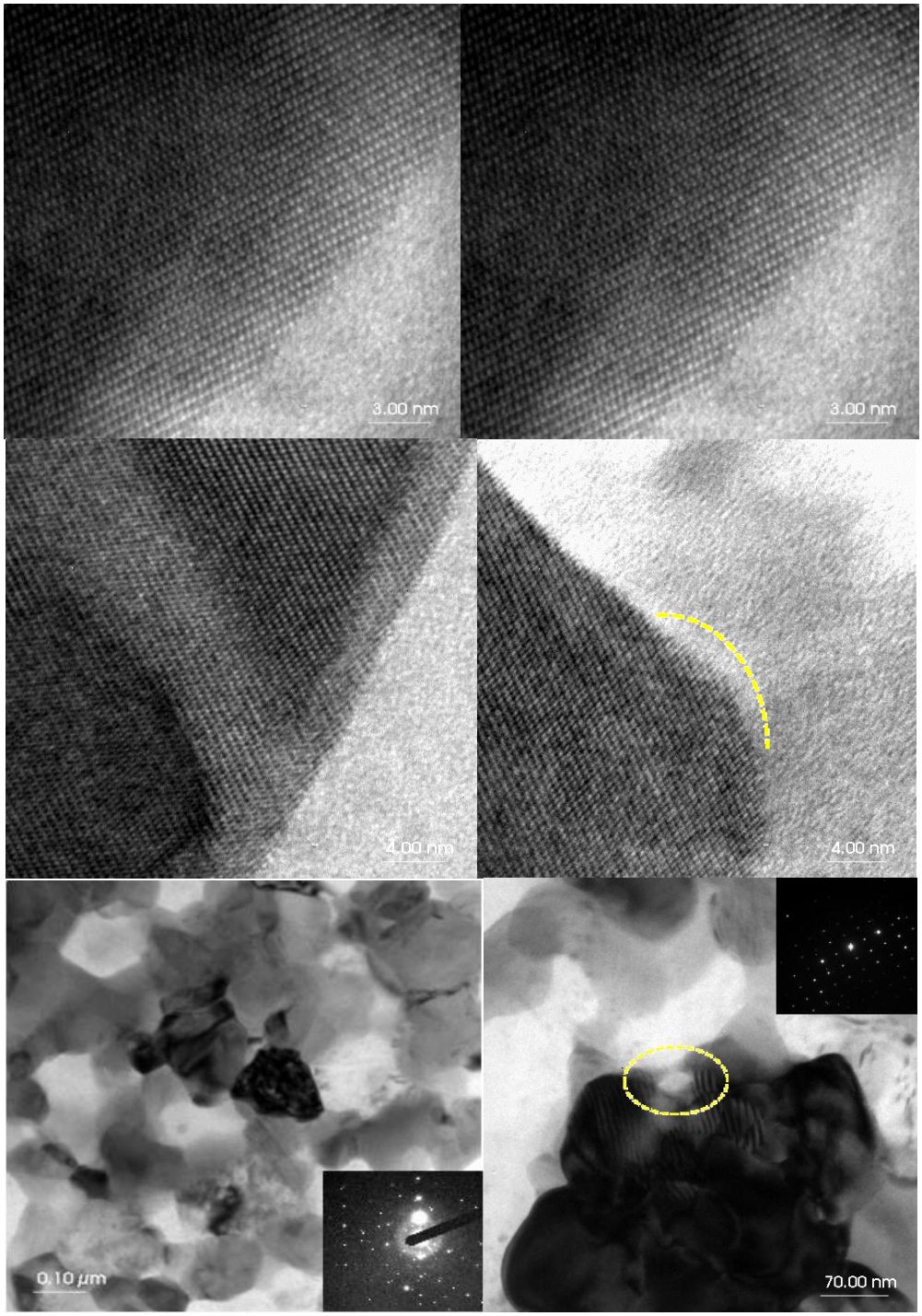

Fig. 5. HREM-images of various sectons of the AMAs tape $Al_{87}Gd_5Ni_4Fe_4$ annealed for 60 min. at T_3 = 645±5 K. (Scale shown in images).

HREM-images, an amorphous matrix with a low concentration of all components is formed between the crystals. The bonds between the crystals are weak, and a loose structure with low mechanical properties is formed. Therefore, annealing for 60 min. does not strengthen the AMAs and leads to a decrease in all mechanical parameters.

Conclusions

X-ray diffraction analysis showed that the nanostructure is formed in the alloys after 5 minutes of annealing, and after another 15 minutes it leads to the formation of a microcrystalline structure. It is shown that the temperature range, annealing time, and kinetics of crystallization of AMA alloys depend on the elemental composition of AMA (base metal, rare earth and amorphizing alloy additives, and their quantitative ratio). It has been shown that the value of n (crystallization rate) of AMA for the $Al_{87}Y_4Gd_1Ni_4Fe_4$ alloy increases from 1.61 to 2.01. The activation energy for the alloys for iron-containing yttrium-containing AMAs, the activation energy practically does not change during the crystallization process. Thermal modification of AMAs: $Al_{87}Gd_5Ni_4Fe_4$ as a result of heat treatment of AMAs from

5 to 15 min., the microhardness increases from 0.20 to 2.75 GPa, and when heat treated for 60 min at a temperatures of T_3 = 645±5, 647±5 K, it decreases to 0.35 and 0.45 GPa.

Khrushchyk Khrystyna – PhD student of the Department of Physics and colloid chemistry of the Faculty of Chemistry of the Ivan Franko National University of Lviv/ Institute of Materials Engineering of the Faculty of Science and Technology of the University of Silesia in Katowice
Barylski Adrian – PhD of the Institute of Materials Engineering of the Faculty of Science and Technology of the University of Silesia in Katowice
Aniolek Krzysztof – PhD of the Institute of Materials Engineering of the Faculty of Science and Technology of the University of Silesia in Katowice
Karolus Malgorzata – D.Sc. of the Institute of Materials Engineering of the Faculty of Science and Technology of the University of Silesia in Katowice
Boichyshyn Lidiya – D.Sc. of the Department of Physics and colloid chemistry of the Faculty of Chemistry of the Ivan Franko National University of Lviv.

[1] A. Inoue, S. Sobu, D. V. Louzguine, H. Kimura, & K. Sasamori, *Ultrahigh strength Al-based amorphous alloys containing*, Sc. J. Mater. Res., 19, (2004); https://doi.org/10.1557/JMR.2004.0206.
[2] A. Inoue, N. Matsumoto, & T. Masumoto, *Al–Ni–Y–Co Amorphous alloys with high mechanical strengths, wide supercooled liquid region and large glass-forming capacity*, Mater. Trans., (1989); https://doi.org/10.2320/matertrans1989.31.493.
[3] A. Inoue, *Amorphous, nanoquasicrystalline and nanocrystalline alloys in Al–based systems*, Progr. Mat. Sci., 43, 365 (1998); https://doi.org/10.1016/S0079-6425(98)00005-X.
[4] W Li, L.T. Kong, J.F. Li. *Thermal stability and crystallization behavior of $Al_{86}Ni_9Y_5$ amorphous alloys with different Si addition*, Mater. Charact., 194, 112387 (2022); https://doi.org/10.1016/j.matchar.2022.112387.
[5] L.M. Boichyshyn, K.I. Khrushchyk, M.O Kovbuz., et al. *Specific Features of the Transition of Amorphous $Al_{87}REM_5Ni_8(Fe)$ Alloys Into the Crystalline State Under the Influence of Temperature*, Mater. Sci., 55(1), 17 (2019); https://doi.org/10.1007/s11003-019-00246-7.
[6] Jiaojiao Yi, Liqiao Yue, Rongjie Xue, Yin Wang, et al. *Mechanism underlying two-step separated fcc-Al crystallization in Al-based metallic glasses*, Mater. Lett., 15, 130488 (2021); https://doi.org/10.1016/j.matlet.2021.130488.
[7] Shuo Zhang, Kai Chong, Zhibin Zhang. *Crystallization behavior and corrosion resistance of $Al_{86}Ni_{10}Zr_4$ amorphous alloy under different annealing treatment conditions*, J. Non Cryst. Solids., 593(1), 121775 (2022); https://doi.org/10.1016/j.jnoncrysol.2022.121775.
[8] S. I. Mudry, Yu. O. Kulyk, L. M. Boichyshyn. *Nanocrystallization of amorphous alloys $Al_{87}Ni_8Dy_5$ indused by head treatment*, Mater. Today: Proc., 62, (2022); https://doi.org/10.1016/j.matpr.2019.08.025.
[9] Michael C. Gao, G.J. Shiflet. *Devitrification sequence map in the glass forming Al–Ni–Gd system*, Scr. Mater., 53(10), 1129 (2005); https://doi.org/10.1016/j.scriptamat.2005.07.021.
[10] W.T. Kim, M. Gogebakan, B. Cantor, *Heat treatment of amorphous $Al_{85}Y_5Ni_{10}$ and $Al_{85}Y_{IO}Ni_5$ alloys*, (1997) Mater. Sci. Eng., 226228, (1997);
[11] J.J. Yi, L.T. Kong, M. Ferr,et al, *Origin of the separated α-Al nanocrystallization with Si added to $Al_{86}Ni_9La_5$ amorphous alloy*, Mater. Charact., 178, 111199 (2021); https://doi.org/10.1016/j.matchar.2021.111199.
[12] J. Q. Wang, H. W. Zhang, X. J. Gu, K, et al, *Identification of nanocrystal nucleation and growth in $Al_{85}Ni_5Y_8Co_2$ metallic glass with quenchedin*, Appl. Phys. Lett. ,80, 3319 (2002); https://doi.org/10.1063/1.1476388.
[13] H. W. Sheng, Y. Q. Cheng, P. L. Lee, et al, *Atomic packing in multicomponent aluminum-based metallic glasses*, Acta Mater., 56, 6264 (2008); https://doi.org/10.1016/j.actamat.2008.08.049.
[14] Y. E. Kalay, I. Kalay, J. Hwang, et al, *Local chemical and topological order in Al-Tb and its role in controlling nanocrystal formation*, Acta Mater., 60, 994 (2012); https://doi.org/10.1016/j.actamat.2011.11.008.
[15] K. Khrushchyk, L. Boichyshyn, V. Kordan, *Influence of annealing on mechanical properties of alloys of Al-REM-Ni(Fe)*, Mater. Today: Proc., 62, 5739 (2022); https://doi.org/10.1016/j.matpr.2022.02.343.
[16] M. Avrami, *Kinetics of phase change. I General theory*, J. Chem. Phys., 7, (1939); https://doi.org/10.1063/1.1750380.
[17] J.A.Augis. *Calculation of the Avrami parameters for heterogeneous solid state reactions using a modification of the Kissinger method*, J. Thermal Anal., 13, 283 (1978); https://doi.org/10.1007/bf01912301.
[18] S.H. AlHeniti, *Kinetic study of nonisothermal crystallization in $Fe_{78}Si_9B_{13}$ metallic glass*, J. Alloys Compd., 484, 177 (2009); https://doi.org/10.1016/j.jallcom.2009.05.07.6.
[19] B. Adnadevic, B. Jankovic, D.M. Minic. *Kinetics of the apparent isothermal and nonisothermal crystallization of the αFe phase within the amorphous $Fe_{81}B_{13}Si_4C_2$*, J. Phys. Chem. Sol., 71 (7), 927 (2010); https://doi.org/10.1016/j.jpcs.2010.04.009.
[20] Y. Yinnon, D.R. Uhlmann, Applications of the thermoanalytical techniques to the study of crystallization kinetics in glassforming liquids, part I: Theory, J. NonCryst. Sol, 54(3), 253 (1983); https://doi.org/10.1016/0022-3093(83)90069-8.
[21] M. Vasic, D.M. Minic, V.A. Blagojevic, *Mechanism and kinetics of crystallization of amorphous $Fe_{81}B_{13}Si_4C_2$ alloy*, Thermochim. Acta, 572, 45 (2013); https://doi.org/10.1016/j.tca.2013.09.027.

[22] Young RA ,*The Rietveld method*, (1993); Oxford University Press
[23] L.B. McCusker, R.B. Von Dreele, D.E. Cox, D. Louër, P. Scardi, *Rietveld refinement guidelines*, J. Appl. Crystallogr, 32, 36 (1999); https://doi.org/10.1107/S0021889898009856.
[24] Wiliamson GK, Hall WH (1953) Acta Metall 1:22.
[25] S. Ahmadi, H.R. Shahverdi, S. S. Saremi, *Nanocrystallization of α – Fe crystals in $Fe_{52}Cr_{18}Mo_7B_{16}C_4Nb_3$ bulk amorphous alloy*, J. Mater. Sci. Technol., 27(6), 497 (2011); https://doi.org/10.1016/S1005-0302(11)60097-2.
[26] D.M. Minic, A. Maricic, B. Adnadevic. *Crystallization of αFe phase in amorphous $Fe_{81}B_{13}Si_4C_2$ alloy*, J. Alloys Compd., 473 (1-2), 363 (2009); https://doi.org/10.1016/j.jallcom.2008.05.087.
[27] A.H. Moharram, M. Abu El-Oyoun, M. Rashad. Crystallization kinetics of two overlapped phases in $As_{40}Te_{50}In_{10}$ glass, Thermochim. Acta., 555, 57 (2013); https://doi.org/10.1016/j.tca.2012.12.019.
[28] D. Janovszky, M. Sveda, A. Syncheva, et al, *Amorphous alloys and differential scanning calorimetry (DSC)*, J. Ther. Anal., 147, 7141 (2021); https://doi.org/10.1007/s10973-021-11054-0.
[29] Si P, X. Bian, W. Li, J. Zhang, Z. Yang, *Relationship between intermetallic compound formation and glass forming ability of Al–Ni–La alloy*, Phys. Lett. A., 319 (3-4), 424 (2003); https://doi.org/10.1016/j.physleta.2003.10.060.
[30] R. Babilas, K. Mlynarek-Zak, W. Lonski, Et al, *Study of crystallization mechanism of Al-based amorphous alloys by in-situ high temperature X-ray diffraction method*, Sci. Rep., 12(1), (2022); https://doi.org/10.1038/s41598-022-09640-9.
[31] T. Mika, M. Karolus, G. Haneczok, L. Bednarska, E. Lagiewka, B. Kotur, *Influence of Gd and Fe on crystallization of $Al_{87}Y_5Ni_8$ amorphous alloy*, J. Non-Cryst. Sol., 354 (27), 3099 (2008); https://doi.org/10.1016/j.jnoncrysol.2008.01.020.

Христина Хрущик[1,2], Адріан Барильські[2], Криштоф Аніолек[2],
Малгоджата Каролус[2], Лідія Бойчишин[1]

Механічні властивості аморфних металевих сплавів системи $Al_{87}(Ni,Fe)_8(REM)_5$ після короткочасного відпалу

[1]*Львівський національний університет імені Івана Франка, Львів, Україна,*
[2]*Сілезький університет в Катовіцах, Катовіце, Польща, krystyna.khrushchyk@us.edu.pl*

Методом диференціальної скануючої калориметрії (ДСК) визначено температури фазових переходів аморфних металів на основі алюмінію $Al_{87}(Ni,Fe)_8(REM)_5$. За допомогою кінетичних моделей (модель Матусіта) передбачено механізми утворення та росту нанокристалів в аморфній матриці. Встановлено, що після відпалу при температурі стабільного росту нанокристалів утворюється рентгенаморфна структура з об'ємною часткою невпорядкованих нанокристалічних фаз твердого стану Al(X), $GdFe_2$, $AlFe_2Ni$, $GdFe_2$ для аморфного металевого сплаву (АМС). Утворюється сплав $Al_{87}Y_4Gd_1Ni_4Fe_4$ та мікрокристалічні фази твердого стану Al(X), $GdFe_2$ $AlFe_2Ni$ для сплаву $Al_{87}Gd_5Ni_4Fe_4$, що істотно впливає на механічні властивості системи $Al_{87}(Ni,Fe)_8(REM)_5$. Досліджено вплив відпалу на механічні властивості аморфних сплавів на основі алюмінію за допомогою методів модуля Олівера-Фарра та Юнга. Встановлено, що термічна модифікація АМС: $Al_{87}Gd_5Ni_4Fe_4$ в результаті термообробки АМС від 5 до 15 хв, мікротвердість зростає від 0,20 до 2,75 ГПа, а при термічній обробці протягом 60 хв за температур T_3 = 645±5 , 647±5 К зменшується до 0,35 і 0,45 ГПа, відповідно.

Ключові слова: аморфні металеві сплави на основі алюмінію, диференціальна скануюча калориметрія, мікротвердість, нанокристалізація, модуль Юнга.